



**AIAA-2003-0916**

## **Progress Towards Real-Time Planar Doppler Velocimetry**

B. Thurow, J. Hileman, M. Samimy and W. Lempert  
The Ohio State University

**41<sup>st</sup> AIAA Aerospace Sciences Meeting and  
Exhibit**

**January 6-9, 2003/ Reno, NV**

## PROGRESS TOWARDS REAL-TIME PLANAR DOPPLER VELOCIMETRY

B. Thurow<sup>1</sup>, J. Hileman<sup>2</sup>, M. Samimy<sup>3</sup> and W. Lempert<sup>4</sup>  
 Dept. of Mechanical Engineering  
 The Ohio State University

**A pulse burst laser and two ultra-high speed digital cameras are incorporated into a planar Doppler velocimetry (PDV) experiment in a first step of the development of real-time PDV. Preliminary experiments conducted on a Mach 2.0 axisymmetric free jet revealed the capabilities and potential of the technique while uncovering problems that must be dealt with. Resulting measurements from the real-time PDV experiment showed expected magnitudes and trends within the average velocity and turbulence intensity profiles. A limiting factor in the experiments was the frequency drift of the pulse burst laser likely due to thermal fluctuations within the phase conjugate mirror. This issue and others are discussed along with potential solutions.**

### I. Introduction

PDV is a powerful optical diagnostic technique that can measure all three instantaneous components of velocity over a two-dimensional plane within a flow field. This is accomplished by measuring the frequency shift of light as it is scattered by particles contained in the flow field. The Doppler frequency shift,  $\Delta f_d$ , is related to the fluid velocity by,

$$\Delta f_d = \frac{(\vec{s} - \vec{o}) \cdot \vec{V}}{\lambda} \quad (1)$$

where  $\vec{s}$  is the unit vector in the direction of the scattered light,  $\vec{o}$  is the unit vector in the direction of the incident laser light,  $\lambda$  is the wavelength of the light and  $\vec{V}$  is the velocity vector of the flow.

The idea of measuring the Doppler shift was originally utilized by Cummins et al. (1964) and Yeh and Cummins (1964). More recently, Komine and Brosnan (1991) and Meyers and Komine (1991) developed a velocimetry technique referred to as Doppler global velocimetry (DGV) that used a molecular filter to measure the Doppler shift and thus the velocity. Since then, this technique has been further developed by numerous research groups including, but not limited to, Elliott et al. (1994), Arnette et al. (1996), McKenzie (1996), Smith et al. (1996), Clancy et al. (1997, 1999), Beutner et al. (1999), Mosedale et al. (2000) and Crafton et al. (2001). In the course of development, many researchers began using the term planar Doppler velocimetry (PDV) to describe the technique.

Today, a typical one-component PDV technique will utilize a pulsed seeded Nd:YAG laser, one or two scientific grade CCD cameras and an iodine filter. The

laser is used to illuminate a plane of the flow with narrow linewidth light. The Doppler shifted scattered light is then split into two using a beamsplitter and imaged by the camera(s), one of which has the iodine filter placed in its path. The absorption of light as it passes through the iodine cell is a function of frequency. Thus, the frequency shift is determined by measuring the amount of light that transmits through the molecular filter. The other image is used as a reference image to accurately determine the frequency shift at every pixel. Complex calibration and image mapping algorithms have also been developed to achieve accuracies as good as 1-2 m/s. More details concerning the history of PDV, the art of its application and recent advances can be found in excellent review articles by Elliott and Beutner (1999) and Samimy and Wernet (2000).

The current limitation on any planar velocity measurement technique including PDV, however, is its inability to acquire time-correlated sets of velocity data in high-speed flows. Commercially available pulsed Nd:YAG lasers are limited to repetition rates on the orders of 10's of Hz and only recently have high-speed digital cameras become commercially available. These factors have limited PDV to instantaneous and average flow measurements. The ability to capture time-sequenced PDV measurements, however, has the potential to reveal characteristics of high-speed flows that currently can only be conjectured. This information could lead to new advances in the understanding and manipulation of high speed flows and their respective applications.

Recently, a pulse burst laser has been developed that can achieve pulse burst repetition rates of up to 1

<sup>1</sup> Graduate student, NDSEG Fellow, member AIAA

<sup>2</sup> Graduate student, OSGC Fellow, member AIAA

<sup>3</sup> Professor, Associate Fellow AIAA, corresponding author: samimy.1@osu.edu

<sup>4</sup> Associate Professor, AIAA Associate Fellow

MHz (Lempert et al., 1996, Wu, et al., 2000 and Thurow et al. 2000, 2001). The laser has been used extensively in conjunction with a high-speed CCD camera in qualitative flow visualization studies by Thurow et al. (2000, 2001a, 2002) and quantitative convective velocity measurements by Thurow et al. (2002). A very preliminary proof-of-concept work by Thurow et al. (2001b) showed the feasibility of using the pulse burst laser and available high-speed cameras to obtain PDV velocity data, but did not measure actual flow velocities.

In this work, we take the first step towards flow measurements using real-time PDV and start the process of the development of a reliable and accurate real-time PDV technique. The main goals of this paper are to understand the current limitations of real-time PDV and to determine methods to deal with these limitations. This is achieved by incorporating the pulse burst laser and two high-speed cameras into a typical and simplified PDV experimental set-up. Section II discusses the specialized equipment used in these experiments and their incorporation into PDV. Basic details concerning the PDV data acquisition and processing are also described in Section II. Section III details the results of the PDV experiment in measuring the velocities of a Mach 2.0 axisymmetric jet. In addition, possible sources of error are discussed as they occur. Section IV discusses these results in more details and suggests a number of feasible changes and additions that can be made to improve the real-time PDV technique. Lastly, section V concludes the paper with a brief summary of the paper's conclusions.

## II. Experimental equipment, arrangement and conditions

### **A. Ultra-high speed equipment**

The three main components of a PDV experiment are a laser, molecular filter and camera. In this set of experiments, both the laser and cameras are specially designed for high-speed applications and therefore offer unique challenges for their incorporation into a PDV experimental set-up. Due to limited availability and high costs, two different ultra-high speed cameras had to be used in this set of experiments.

#### *Pulse burst laser*

The laser, illustrated in Fig. 1, is a second generation system based on that described previously by Lempert et al. (1996), Wu, et al (2000) and Thurow et al. (2000,2001). A continuous wave Nd:YAG ring laser serves as the primary oscillator, the output of which is pre-amplified in a double-pass flashlamp-pumped, pulsed amplifier. The resulting, approximately

150 microsecond duration pulse is formed into a "burst" train using a custom, dual Pockel Cell "slicer". The output of the slicer is further amplified in a series of four additional amplifiers and then converted to the second-harmonic wavelength (0.532 microns) with a Type II KTP Second Harmonic Generation (SHG) crystal. The final output is a flexible "burst" of pulses, with inter-pulse spacing as short as 1 microsecond and individual pulse duration as short as 4 nanoseconds. The number and spacing of the pulses is quite flexible, but is ultimately limited by the  $\sim 100 - 150$  microsecond period for which the flashlamp-pumped amplifiers have significant gain. The repetition rate of the burst sequence is as high as 10 Hz, limited by the thermal loading of the amplifiers.

In the experiment herein, a typical burst consists of 14 pulses separated in time by 6 microseconds each and with an average power of 25 mJ/pulse. The power distribution over a burst of pulses is shown in Fig. 2. More uniform distributions of pulse energies are attainable, but generally at the sacrifice of overall power.

Unlike typical pulsed Nd:YAG lasers with unstable resonator oscillators, the pulse burst laser frequency characteristics are determined by the master oscillator, which uses a continuous wave (cw) ring cavity. The master oscillator is a Lightwave Electronics diode-pumped, non-planar ring laser operating at 1.064 microns. The ring resonator operates at a single mode with bandwidth less than 5 kHz. The output pulses of the pulse burst laser are Fourier transform limited and have a bandwidth of  $\sim 45$  MHz for a 10 nsec pulse at 1.064 microns. The frequency can be tuned by adjusting the voltage input to a thermoelectric cooler contained in the Nd:YAG master oscillator. The tuning coefficient of the laser in between mode hops has been measured to be 9.23 GHz/Volt (Thurow et al., 2001).

Recently we have incorporated a Phase-Conjugate Mirror (PCM) into the burst mode laser amplifier chain in order to minimize the occurrence of amplified spontaneous emission (ASE) and to eliminate the 'DC pedestal' contained in each burst of pulses. ASE and the pedestal propagate through the amplifier chain and rob the pulses of gain and consequently limit the power output of the laser. These objectives are achieved using backward stimulated Brillouin scattering (SBS) produced by the interaction between the incident laser light and the hypersonic acoustic waves of the phase conjugating fluid. The SBS process is non-linear such that only intense laser light will be reflected. Thus, only the high intensity laser pulses will be reflected while the lower intensity ASE and 'DC pedestal' will transmit through the mirror and out of the laser system. Physically, the PCM consists of a 75 mm f.l. lens and an optical quality glass cell filled with FC-75, a

fluorinert fluid manufactured by 3M. The PCM has yielded a power increase by a factor of 3-5 over previous publications. More details concerning the implementation of the PCM into the pulse burst laser are contained in Lempert et al. (2002).

Related to PDV, the SBS also causes a frequency shift and time compression of the reflected laser pulses. The magnitude of these features is determined by the speed of sound within the FC-75 fluid. The frequency shift has been measured to be on the order of +2 GHz and compares well with measurements made by Ni and Kung (1996) on FC104. The magnitude of this shift, however, is dependent upon the speed of sound with the phase conjugating fluid. Therefore, small temperature fluctuations can cause a relatively large shift in the frequency of the laser. The implications of this will be discussed in Sec. III.

The bandwidth increase was not directly measured, but is expected to be primarily due to the pulse compression. The output pulses have a duration of ~5 nsec and thus are expected to have a Fourier transform limited bandwidth of ~90 MHz (180 MHz @ 0.532 microns).

#### *Ultra-high speed camera 1: Dalsa 64K1M*

The Dalsa 64K1M ultra-high speed camera has been used extensively with the pulse burst laser for flow visualization on compressible jets (Thurrow et al., 2000, 2001, 2002). It can capture 17 images with 245 x 245 pixel resolution at framing rates up to 1 MHz. The camera consists of a large format CCD chip (1024 x 1024) where 16 out of 17 pixels are masked from the incoming light. The charge produced at each of the active pixels is then shifted to pixels underneath the mask for storage with appropriate timing to produce frame rates up to 1 MHz. Each active pixel has an aperture of 9.5 x 9.5 microns with a pitch of 57.7 microns resulting in a fill factor of <3%. Combined with a quantum efficiency of <10% at 0.532 microns, the light receptivity of the camera is quite low.

To increase the overall data acquisition rate, the data is read out from the CCD in four separate columns at 10 MHz/column. Each column will have its own associated gain and noise characteristics. The output signal can have a video gain of either 1 or 4 and is 12-bit digitized. The dynamic range of the camera is 67 dB and has a dark noise of ~1.5 intensity units. In terms of PDV, the camera's small pixels, low receptivity and small dynamic range are less than ideal and present a challenge in practice.

#### *Ultra-high speed camera 2: PSI IV*

The 2<sup>nd</sup> camera used in these experiments is manufactured by Princeton Scientific Instruments (PSI). This camera can acquire 28 images with a resolution of 82 x 161 pixels. High frame rates are achieved by

shifting charge produced by the pixels to 28 individual memory modules contained next to each pixel. This is similar in operation to the Dalsa camera, however, the storage modules have a much smaller area than the active area of the pixel resulting in a fill factor of almost 50%. Furthermore, each pixel has active dimensions of ~115 x 55 microns. Thus, the camera is much more receptive to light than the Dalsa camera. The dynamic range of the signal is ~74 dB and the full well depth is 60,000 electrons.

Unfortunately, approximately 20% of the pixels on the CCD chip are damaged and unusable. These pixels, however, are predominantly located on one half of the CCD array. Therefore, only an 82 x 82 portion of the chip was found useful in this set of experiments.

## **B. Experimental Facility and Arrangement**

### *Mach 2.0 Jet facility*

The flow field under consideration is a Mach 2.0 axisymmetric ideally expanded jet. The diverging contour of the nozzle was designed using the method of characteristics for uniform flow at the nozzle exit. The exit diameter is 2.54 cm (1"). Air is supplied to the stagnation chamber from two four-stage compressors; it is filtered, dried and stored in two cylindrical tanks with a total capacity of 42.5 m<sup>3</sup> at 16.5 MPa (1600 ft<sup>3</sup> at 2500 psi). The core velocity of the jet is ~500 m/s assuming isentropic expansion of the air through the nozzle. For flow seeding, acetone is injected approximately 15 m upstream of the nozzle to allow adequate time to evaporate before reaching the stagnation chamber. As the flow expands, the associated temperature drop causes the evaporated acetone to condense into small sub-micron droplets that scatter the incident laser light. Additional sub-micron droplets of condensed water are also formed within the mixing layer as the jet entrains moist ambient air. The signal from water condensation, however, is an order of magnitude lower than the acetone signal as the experiments were conducted in December on a cold day with low humidity. Experiments conducted on hot and humid days yield a much larger amount of product formation within the mixing layer.

### *PDV Experimental arrangement*

The experimental arrangement is shown schematically in Figure 3 with an accompanying photograph in Figure 4. The arrangement is typical of a one-component/two-camera PDV experiment and consists of two cameras (filtered and reference), a beam splitter and an iodine cell. Due to time constraints and the preliminary nature of this experiment, some common elements of a PDV system such as a frequency monitoring system and polarizers in front of the cameras were not incorporated. Furthermore, two

additional beam splitters are used to reduce the signal intensity of the filtered image as ND filters were not available at run time. The adverse effects of the missing PDV elements and the unconventional use of the beam splitters is recognized and will be discussed in section IV. Future experiments, however, will allow for more complexity and will incorporate these elements into the system.

The pulse burst laser beam was formed into a laser sheet using two cylindrical lenses located  $\sim 40$  cm from the center of the jet resulting in a maximum spread angle of 6 degrees over the imaging region. The laser sheet formed a 45 degree angle with the jet axis, intersecting it at 5 jet diameters downstream. The imaging system was placed perpendicular to the laser sheet. The resulting velocity sensitivity vector is thus along the axis of the jet as shown in Figure 3. This orientation was chosen so that the system would be sensitive to the most dominant (u) velocity component of the jet and thus large frequency shifts could be expected. The measured velocity field will consist entirely of the u velocity component with an expected frequency shift of 1.3 GHz for the 500 m/s jet core flow.

Due to its high sensitivity and larger dynamic range, the PSI camera was chosen to acquire the filtered image. A f/# 2.8 80-200 mm f.l. zoom lens was used for imaging. The reference image was acquired by the Dalsa camera with light reflected from the beamsplitter. A f/# 1.8 100 mm f.l. lens was used for imaging with the Dalsa camera. Each camera visualized a 5 x 5 cm region. At uniform illumination, however, the signal recorded on the PSI camera was almost two orders of magnitude larger than that recorded by the Dalsa camera. Due to the limited dynamic range of both cameras, this limited the signal levels on the reference camera to very low values. In order to equalize the sensitivity of the two cameras, two beam splitters were placed in the path of the filtered image (PSI camera) and the f/stop was reduced to f/# 4 reducing the incoming light intensity to the PSI camera by a factor of  $\sim 8$ . Despite these steps, the PSI camera signal was still significantly higher than the Dalsa camera. Neutral density (ND) filters were not used as none were available within the time constraints of this experiment. The adverse effects of using beam splitters and a higher f/stop will be discussed later. Future experiments will circumvent these issues through the use of ND filters.

### C. General PDV details

#### *Iodine cell and laser frequency calibration*

The iodine cell in the experimental set-up is 10 cm in length and 10 cm in diameter. It was prepared with an iodine partial pressure of 4.28 torr and pressure broadened with Nitrogen at 41 torr. Electric heating

tape surrounds the cell and is used to keep the cell's temperature at approximately 130 °C. The cell was calibrated by placing a water tank at the object plane of the PDV system. Coffee creamer particles were dissolved in the water and used as scattering particles for illumination of the laser sheet. The particles are small enough that they cannot be individually imaged, but large enough to scatter enough light to both cameras. The laser was then tuned through a 20 V range and the transmission ratio was measured. The resulting transmission profile was then compared with the theoretical transmission profile as determined from the widely used code of Forkey (1996) to determine the tuning range (2<sup>nd</sup> harmonic) of the pulse burst laser.

The tuning range of the pulse burst laser was found to be from 18787  $\text{cm}^{-1}$  to 18789.5  $\text{cm}^{-1}$ , or a total range of 75 GHz. The tuning coefficient of the laser in between mode hops is 9.23 GHz/V. For these experiments, the absorption feature located at 18787.8  $\text{cm}^{-1}$  was used to determine the Doppler shift of scattered light from the jet. Figure 5 is plot of the transmission of this absorption well versus tuning voltage. The laser was set at  $-1.94$  V for the jet experiments with an expected frequency shift of  $\sim 0.14$  V (1.3 GHz) for jet core fluid. Thus the high velocities of the jet would result in a transmission ratio through the filter of  $\sim 0.7$ . The frequency shift of the profile indicated in the figure will be discussed in the next section.

#### *Image registration and processing*

Image matching between the two cameras was achieved using a standard dot card placed at the imaging plane. The dot card consisted of 0.5 mm dots evenly spaced 5.08 mm apart in a square grid pattern. The dot size was specifically chosen so that both cameras would image the dots with multiple pixels despite their different resolutions. Dot card images were obtained before and after the running of the jet to make sure nothing moved during the run.

Image processing and mapping was conducted using a combination of Matlab and a PDV software package purchased from Innovative Scientific Solutions Inc. Due to the large differences in resolution between the two cameras (82 x 82 vs 245 x 245), images from the PSI camera were initially resized to 246 x 246 pixels. Both images were later reduced to the lesser resolution of the PSI camera. By increasing the size of the PSI images as opposed to decreasing the size of the Dalsa images, the full dot card information recorded on the Dalsa image can be retained while keeping both images at similar resolutions. This step should result in better alignment between the two images. The PDV software was then used to find the center of all the dots in both images and create a set of 'tie' points for mapping the Dalsa and PSI images to a common

coordinate system. In the mapping step of all the images, a 3 x 3 binning filter was used to reduce the image resolution back to the lower resolution of the PSI camera.

Mapped images have a 63 x 63 resolution and view a 45.7 x 45.7 mm area of the flow. The effects of mapping can be seen in Figures 6-9. Figure 6 is a raw image of the jet from the Dalsa camera. The image appears quite noisy with the intensity variation in the middle being 10% of the mean (NSR=0.1). The noise is believed to be primarily due to a type of image noise associated with coherent laser light termed 'speckle' noise. Speckle noise to signal ratio (NSR) can be calculated (Arsenault and April, 1976 & Smith, 1998) from

$$NSR \sim (\lambda f/\#)/\Delta x \quad (2)$$

where  $\lambda$  is the wavelength of laser light,  $f/\#$  is the ratio of focal length to aperture of the lens and  $\Delta x$  is the pixel size. For the small pixels of the Dalsa camera this value is 0.1, in agreement with the apparent image noise, indicating that the image noise is mainly speckle limited. Figure 7 is a raw image from the PSI camera and has a NSR of about 0.04. The expected speckle noise is 0.03, which is still in good agreement with the value obtained from Equation 2. Figures 8 and 9 are the mapped images. The images were not low-pass or median filtered at any point in the process. The 3 x 3 binning filter, however, had a net smoothing effect on the Dalsa images lowering the NSR in the center of the jet. This filter had minimal effect on the PSI images, which were first resized to a larger format and then rescaled close to their original size by the binning. Figures 8 and 9 also show the subpixel accuracy of the image registration software as the images match up very well on the same coordinate system.

#### *Flatfield Calibration*

Flatfield calibration of the PDV system was determined by placing the water tank at the object plane of the two cameras in the same manner as the filter profile calibration procedure. The laser was then tuned to a location of maximum transmission through the iodine filter and images acquired at various power settings. Fifty sets of images were obtained before the running of the jet and 50 sets of images afterwards. The flatfield image is especially important and challenging in these experiments due to the very different cameras being used as well as the four column readout process of the Dalsa camera. Figure 10 is an image of the flat field correction slopes. The intensity value at each pixel is multiplied by the corresponding intensity value at the same pixel location of the Dalsa camera so that each image has an equal response to the same intensity input. Figure 10 contains some sharp gradients corresponding to the different readout regions of the Dalsa camera. The figure also has a few rows of

pixels on the right hand side that are affected by the damaged portion of the PSI CCD chip. The features of this calibration image will be quite important in the data reduction portion of the experiment.

#### **D. Jet experiments**

The PDV apparatus described above was used to acquire 100 sets of data of a Mach 2.0 axisymmetric jet. The pulse burst laser was set to produce 14 pulses separated by 6 microseconds each with an average power of ~25 mJ/pulse. A filter profile was acquired beforehand using the procedure detailed in Sec. 2C. Immediately following the acquisition of the filter profile, 100 image sequences were taken of the jet operated in ideally expanded flow regime. This was immediately followed by another filter profile. Also, flat field calibration images and dot card images were also acquired before and after the running of the jet.

The PSI camera was set to take an image every 3 microseconds, leaving a dark image in between each image of the jet. The Dalsa camera took an image every 6 microseconds with the last 3 images (of the sequence of 17) being dark. Dark images were intentionally captured to investigate if any charge from previous images would 'spill' over into subsequent images. As long as the intensity remained below each camera's maximum, this was not a problem. If a camera did saturate, however, the saturated portion of the image would 'bleed' to subsequent images. Saturation was avoided in these experiments.

### III. Experimental Results

The results presented here are preliminary and intended to elucidate some of the issues associated with the development of real-time PDV. Therefore, the main emphasis will be on the improvement of the technique with analysis of the actual velocity results only being a secondary focus. Future studies will correct the problems found in this study and will concentrate more on the actual results.

First, we would like to look at the filter profiles obtained before and after the jet experiments. These two profiles were taken about 30 minutes apart and are shown in Figure 5. During this time, the laser frequency drifted over 400 MHz. The shape of the profiles, however, is quite similar, particularly over the linear range of the curve. The large frequency drift was quite unexpected and made analysis of the jet results more challenging. Similar experiments conducted in the past with the pulse burst laser without the phase conjugate mirror (Thurrow et al., 2001) did not reveal this problem. Furthermore the expected frequency drift associated with master oscillator of the pulse burst laser is expected to be less than 50 MHz/hour. Therefore, it is believed that this drift is a result of the phase

conjugate mirror and the associated SBS process. The frequency shift of the laser light is a function of the speed of sound within the phase conjugating fluid, which is a function of temperature. Thus, the frequency shift will largely be sensitive to small temperature fluctuations within the room and fluid. Figure 11 is a plot of the associated frequency jitter. This plot was created in a similar manner to the filter profile except that the tuning voltage was held at a constant value for a transmission ratio of approximately 0.7. Each measurement in Figure 11 is separated by approximately 10 seconds. The magnitude of the jitter is .028 (3.6% of the expected value). It is expected that this number would grow larger over longer periods of time due to long term drift as evidenced by the filter profiles. Insulating the PCM may be an effective solution to minimizing this frequency drift, but clearly a frequency monitoring system is necessary to monitor the frequency changes. Active control of the PCM temperature may also be necessary to stabilize the laser frequency.

Figure 12 is a pulse to pulse measurement of the frequency jitter within a single burst of pulses. There is some slight variation in the measured transmission ratio, however, it is much lower than the burst to burst fluctuations. It is unclear if the pulse-to-pulse variations is an actual frequency change or due to low signal levels and a less than ideal flat field correction. The transmission through the filter appears to be quite constant for pulses 2-7 where the pulse energy levels are the highest. Nonetheless, a frequency monitoring system would clarify this.

Despite this problem with the frequency stability, the jet data was still analyzed using both filter profiles as well as an in-situ frequency monitoring system. The results obtained using either filter profile are expected to be in error as the laser's frequency changed between their respective acquisitions. As the laser frequency was not known directly, an in-situ frequency monitoring method was implemented. The in-situ frequency monitoring system is based on the assumption that the jet core would have a velocity of ~500 m/s (isentropic expansion value) and therefore the average ratio within the jet core would correspond to this value. The filter profile would then be shifted such that a 1.33 GHz shift (0.144 V in Fig. 5) from the laser set point of -1.94 V would yield a ratio equal to the average ratio of the jet core in the first image (out of a sequence of 14). While not ideal for absolute velocity measurements, the in-situ frequency monitoring system will provide for adequate velocity fluctuation measurements as long as the frequency drift does not extend measurements beyond the linear part of the filter profile. In these experiments, this will be true for the higher velocities of the jet core. At lower velocities,

however, a mismatch between the in-situ determined frequency and the actual frequency can lead to errors.

Figure 13 is an instantaneous velocity image of the flow using the in-situ frequency monitoring system. The axis units are in pixels and the measured velocity is the u component of velocity at that point. Remember that the sheet is at 45 degrees with respect to the jet axis. The image is oriented such that the left hand portion of the image is further upstream and the downstream location increases as you move to the right. The velocity at the center is by definition 500 m/s as it was set there with the in-situ frequency monitoring. As expected, the velocity decreases as one moves away from the center of the jet. The fluctuation of velocities within the jet core has a magnitude of ~ 25 m/s (5% of mean), which agrees well with expected turbulence intensities as measured in a similar Mach 2.0 jet by Clancy et al. (1999).

In Fig. 13, the lowest measured value of velocity is approximately 350 m/s. The predominant reason for this is the laser frequency fluctuations. Velocity values below 300 m/s begin to correspond to the non-linear portion of the filter profile where the absorption is near its maximum. Thus, a less than ideal signal level is being measured for these velocities. Another reason for this is the low signal levels of the reference image within the mixing layer. The acetone condensation seeding technique predominantly marks the core of the jet and decreases in concentration away from the jet core. Typically this loss of signal is offset by the condensation of water into the mixing layer as it is entrained from the moist ambient air. In this set of experiments, however, being conducted in December, this effect was minimal. The combined effects of the frequency drift, a cold day and a low sensitivity reference camera make adequate visualization of the mixing layer difficult. The biggest problem, however, is felt to be the laser frequency drift, which we believe can be adequately corrected to extend measurements outside of the jet core.

Figures 14 and 15 present low pass filtered three-dimensional surface plots representing the average velocity and turbulence fluctuations, respectively. The statistics were calculated using 100 sets of images with velocities calculated using the in-situ frequency monitoring. The shape of the figures remains the same using either of the filter profiles in Figure 5, however, the magnitudes change. Figure 13 exhibits a fairly flat velocity profile across the jet core. This agrees well with PDV and LDV measurements made on a similar Mach 2.0 jet by Clancy et al (1999) which showed a 'top hat' profile at these locations. The velocity fluctuations of Figure 14 also exhibit the expected shape where the fluctuations are highest within the mixing layer. It should be noted that only pixels where a frequency shift could be measured were include in the

statistical measurements. Default values of 0 m/s were not included in the measurements.

Table 1 lists the mean velocity  $V_x$  values and the normalized turbulence intensities,  $V_x'/V_x$  (jet core and mixing layer). The table lists these values as calculated using the pre-experiment filter profile, post-experiment filter profile, in-situ frequency monitoring and the values measured by Clancy et al (1999). From these values, it appears that the frequency of the laser was closer to the post-exp filter than the pre-exp filter during run time. The in-situ method of frequency filtering as well as the post-exp filter profile produce relative statistics on par with the measurements of Clancy et al. (1999).

While the data is too preliminary to make any definitive statements concerning its accuracy, the measured velocity fluctuations within the jet core and the mixing layer are encouraging. The velocity fluctuations in the mixing layer are likely in error due to a limited sensitivity range of only 300 to 500 m/s, which would result in lower fluctuation levels. On the other hand, the lower signal levels within the mixing layer are a source of noise in the measurements that seems to statistically offset the bias towards lower fluctuation levels. The jet core data was produced with both cameras registering relatively high signal levels and is believed to be more accurate. The high levels of core fluctuations for the pre and post-experiment filters is likely due to the frequency drift that occurred during the runs. This drift artificially adds fluctuations to the velocity from one image set to the next when the frequency is not monitored.

#### IV. Discussion of results and sources of error

The experiments described in this paper are the first step towards obtaining high quality real-time PDV data. The goal of this paper was to identify problems associated with the equipment used and to determine actions that can be taken to alleviate these problems. These problems and potential solutions are discussed here.

The largest source of error in the current experimental apparatus appears to be the frequency drift of the laser due to the PCM. These drifts occur due to temperature changes within the phase conjugating fluid. The magnitude of these changes can be minimized by active or passive temperature control. A simple means of passive temperature control is to insulate the PCM so as to dampen any temperature fluctuations that may occur due to thermal gradients in the air around the PCM. Active temperature control, however, may be needed to minimize temperature changes due to the laser itself as it focused inside the PCM.

This frequency drift also resulted in the laser being tuned to a region of high absorption within the filter profile when it is desirable to keep the measurements at points of higher transmission. This had the adverse effect of causing low frequency shift measurements to result in very low transmission ratios. At low transmission ratios, the signal cannot be distinguished from the background and any measurements made in this area are noise-dominated. Thus, in the current experiments, only velocities above ~200-300 m/s had a high enough transmission to substantially rise above the noise. A more stable frequency of the laser would greatly alleviate this problem by ensuring that the laser frequency is set so that all velocities would result in a filter transmission above the noise level. A frequency monitoring system can also be used to track the frequency drift and jitter that occurs and accurately calibrate each data point to the laser frequency.

A second source of error is the low signal levels recorded within the mixing layer of the jet. As mentioned, this is a combination of the water content in the air (very low for these experiments), low laser powers and a low sensitivity camera. Much larger signals within the mixing layer are obtainable on hot and humid summer afternoons. Thus, appropriate facility scheduling may alleviate much of the problem. Another solution would be to add more amplifiers to the pulse burst laser system. This could potentially increase the power of the laser by a factor of 2-5. The problem with this solution is the added complexity and cost this would add to the laser system as it would require additional cooling capacity and possibly necessitate a splitting and recombining of the laser pulses to avoid gain saturation within the laser crystals. More power can also be obtained by using fewer pulses with larger pulse separations. Finally, low signal levels can be alleviated by using different seeding techniques. The current facility allows for the addition of a low-speed co-flow. This co-flow could be utilized and seeded with particles to provide a more filled out imaging field that is less dependent upon mixing and has a more uniform seeding density.

An additional problem that can be seen in the average velocity images (difficult to see in Fig. 13) is that the average velocity image contains many of the same characteristics as the flat field correction (see Fig. 10). As mentioned, the Dalsa camera is read out in 4 individual columns, each of which will carry its own level of noise and sensitivity. This added complexity produces sharp gradients within the flat field corrections and places a premium on its accurate determination. The velocity in the jet core has these same features as sharp gradients are present at the same locations.

In the current flat-field calibration, a water tank is seeded with small creamer particles providing a particle

field to scatter light from the laser sheet. An inherent disadvantage to this system is that instantaneous images will contain speckle noise, thus increasing the requirement for a large set of images at different intensity levels. Obtaining the flat field correction in a different manner may help alleviate this problem. One method used by various researchers is to direct the laser light through a fiber optic onto a white card placed within the field of view of the cameras. A diffuse piece of glass is then used to scatter the light and destroy the coherence of the beam. This method helps reduce speckle noise and eliminates problems associated with large particles that may drift into the plane of the laser sheet. The technique also creates a more uniform field of illumination that is more ideal for calibration.

The nature of the light scattering particles is also not fully understood and may lead to errors associated with the laser's polarization. The polarization of scattered light is largely dependent on the size of the scattering particles. Ideally, the beam splitter would equally transmit and reflect light of all polarizations. Practically, however, there is a slight dependence on the polarization. Thus, the size of particles could influence the amount of light being divided among the two cameras. In addition, the current experiment used two additional beam splitters to reduce the signal intensity of the filtered image below saturation. These beam splitters would only serve to multiply the problem. Polarization effects can be eliminated, however, by incorporating a polarizer into experimental set-up so that the cameras only see light of a certain polarization, thus making the reflected and transmitted light of the beam splitter a constant. ND filters can be used in place of beam splitters to reduce the incident intensity on the PSI camera. This too would minimize polarization effects as well as allow a more precise reduction of incident intensity.

## V. Conclusions

The first steps in the development of a real-time PDV system have been taken in this work as potential problems have been highlighted and addressed. The foremost problem of laser frequency drift is similar to problems encountered early on in the development of conventional PDV systems. As is done in the conventional PDV, a frequency monitoring system will be incorporated into future set-ups. In addition, the phase conjugate mirror will be insulated to minimize the temperature fluctuations that are causing this drift. Active temperature control will also be explored. Additional problems arose from the mismatch of camera characteristics (flat field calibration and low reference signal levels). The combined effect of these

problems limited the current set of experiments to only measuring velocities above 300 m/s.

Nonetheless, the statistical results obtained in these experiments are quite encouraging. The average velocity and velocity fluctuation profiles both exhibited expected trends and magnitudes for a Mach 2.0 axisymmetric jet. Furthermore, these measurements had similar results to similar measurements made on another Mach 2.0 axisymmetric jet. Solutions to the problems that limited these results, have been proposed and further refinement of the technique should produce substantially better results.

The next step in the development of real-time PDV will be to implement these solutions and acquire a new set of data. These new experiments will not only resolve the issues discussed here, but will highlight more subtle issues concerning real-time PDV and define the degree of error that is reasonable to expect. These experiments will also produce a reliable set of data that can be used to create numerical models of time varying flow fields (e. g. proper orthogonal decomposition of the flow field). These models can then be used to refine the requirements of the real-time PDV system in terms of accuracy and acquisition rates and will influence the next stage of its development.

Overall, the experiments herein were successful in elucidating the issues confronting PDV. The experiments also demonstrated the potential of PDV to acquire time-correlated sets of velocity data in high-speed flows. The average velocity and velocity fluctuation profiles were quite encouraging as they agreed well with PDV data taken in a conventional manner on a similar jet. Future experiments will be able to analyze the data with respect to its temporal development and will make better use of the time-correlated data.

## Acknowledgments

The first author would like to thank the Department of Defense for his National Defense Science and Engineering Graduate Fellowship. The second author would like to thank the Ohio Space Grant Consortium for his OSGC Doctoral Fellowship. Subin Sethuram is acknowledged for his assistance in these experiments.

## References

- Arnette, S. A., Samimy, M., and Elliott, G.S., "Two-component planar Doppler velocimetry in the compressible turbulent boundary layer," *Exp Fluids*, Vol. 24, 1998, pp. 323-332.
- Beutner, T.J., Williams, G.W., Baust, H.D., Elliott, G.S., Crafton, J., and Carter, C.D., "Characterization and applications of Doppler global velocimetry," AIAA Paper 98-2608, June, 1998.

- Clancy, P.S., and Samimy, M., “Two-component planar Doppler velocimetry in high-speed flows,” *AIAA J.*, Vol. 35, No. 11, 1997, pp. 1729-1738.
- Clancy, P.S., Samimy, M., and Erskine, W.R., “Planar Doppler velocimetry: Three-component velocimetry in supersonic jets,” *AIAA J.*, Vol. 37, No. 6, 1999, pp. 700-707.
- Crafton, J., Carter, C. D., and Elliott, G.S., “Three-component phase-averaged velocity measurements of an optically perturbed supersonic jet using multi-component planar Doppler velocimetry,” *Measurement Science and Technology*, Vol. 12, 2002, pp. 409-419.
- Cummins, H. Z., Knable, M., and Yeh, Y., “Observation of diffusion broadening of Rayleigh scattered light,” *Physical Review Letters*, Vol. 12, No. 6, pp. 150-153, 1964.
- Elliott, G. S., Samimy, M., and Arnette, S. A., “A molecular filter based diagnostics in high-speed flows,” *Experiments in Fluids*, Vol. 18, 1994, pp. 107-118.
- Elliott, G. S. and Beutner, T. J., “Molecular filter based planar Doppler velocimetry,” *Progress in Aerospace Sciences*, Vol. 35, 1999, pp. 799-845.
- Forkey, J.N., “Development and demonstration of filtered Rayleigh scattering- a laser based flow diagnostic for planar measurements of velocity, temperature and pressure,” Final technical report for NASA Graduate student researcher, Fellowship grant #NGT-50826, Princeton University, 1996.
- Komine, H., and Brosnan, S., “Instantaneous, three-component, Doppler global velocimetry,” *Laser Anemometry*, Vol. 1, Aug 1991, pp. 273-277.
- Lempert, W., Thurow, B., Bezant, A., and Samimy, M., “A MHz rate imaging system for study of turbulent and time evolving high speed flows,” 11th International Symposium on Application of Laser Techniques to Fluid Mechanics (Lisbon, Portugal, July 8 – 11, 2002)
- McKenzie, R. L., “Measurement capabilities of planar Doppler velocimetry using pulsed lasers,” *Applied Optics*, Vol. 35, No. 6, 1996, pp. 948-964.
- Meyers, J., and Komine, H., “Doppler global velocimetry: A new way to look at velocity,” *Laser Anemometry*, Vol. 1, Aug. 1991, pp. 289-296.
- Mosedale, A.D., Elliott, G.S., Carter, C.D., and Beutner, T. J., “Planar Doppler velocimetry in a large-scale facility,” *AIAA J.*, Vol. 38, No. 6, June 2000.
- Ni, C.K. and Kung, A.H. (1996), “Effective suppression of amplified spontaneous emission by stimulated Brillouin scattering phase conjugation”, *Optics Letters*, Vol. 21, pp. 1673-1675.
- Samimy, M., and Wernet, M.P., “Review of planar multiple-component velocimetry in high-speed flows,” *AIAA J.*, Vol. 38, No. 4, 2000, pp.553-574.
- Smith, M.W., Northam, G.B., and Drummond, J. P., “Application of absorption filter planar Doppler velocimetry to sonic and supersonic jets,” *AIAA J.*, Vol. 34, No. 3, 1996, pp. 434-441.
- Thurow, B., Lempert, W., and Samimy, M., (2000), Paper AIAA-2000-0659, 38<sup>th</sup> AIAA Aerospace Sciences Meeting, Reno, NV. Jan 10 - 13, 2000.
- Thurow, B., Hileman, J., Samimy, M. and Lempert, W. (2001a), “An In-Depth Investigation of Large Scale Structures in a Mach 1.3 Axisymmetric Jet,” Paper AIAA-2001-0148, 39<sup>th</sup> AIAA Aerospace Sciences Meeting, Reno, NV, Jan. 8 - 11, 2001.
- Thurow, B., Hileman, J., Samimy, M. and Lempert, W., (2001b), “Progress Towards a Real-Time Quantitative Measurement Technique for High Speed Flows, AIAA Paper 2001-2985, 31<sup>st</sup> AIAA Fluid Dynamics Conference, Anaheim, CA, June 11-14, 2001.
- Thurow, B., Hileman, J., Samimy, M. and Lempert, W., (2002), “Compressibility Effects on the Growth and Development of Large-Scale Structures in an Axisymmetric Jet, Paper AIAA-2002-1062, 40<sup>th</sup> AIAA Aerospace Sciences Meeting, Reno, NV, January 14-17,2002.
- Wu, P., Lempert, W. R., and Miles,R.B. (2000), “MHz Pulse-Burst Laser System and Visualization of Shock-Wave/Boundary-Layer Interaction in a Mach 2.5 Wind Tunnel,” *AIAA Journal* 38, pp. 672-679.
- Yeh, Y. and Cummins, H., “Localized fluid flow measurements with a He-Ne laser spectrometer,” *Applied Physics Letters*, Vol. 4, No. 99, 1964, pp. 176-178.

Method	$V_x$	$V'_x/V_x$ (jet core)	$V'_x/V_x$ (mixing layer)
Pre-exp filter profile	275 m/s	.16	.24
Post-exp filter profile	440 m/s	.10	.15
In-situ freq monitoring	500 m/s	.05	.13
Clancy et al. (1999)	500 m/s	.05	.14

Table 1 – Statistical calculations using different filter profiles.

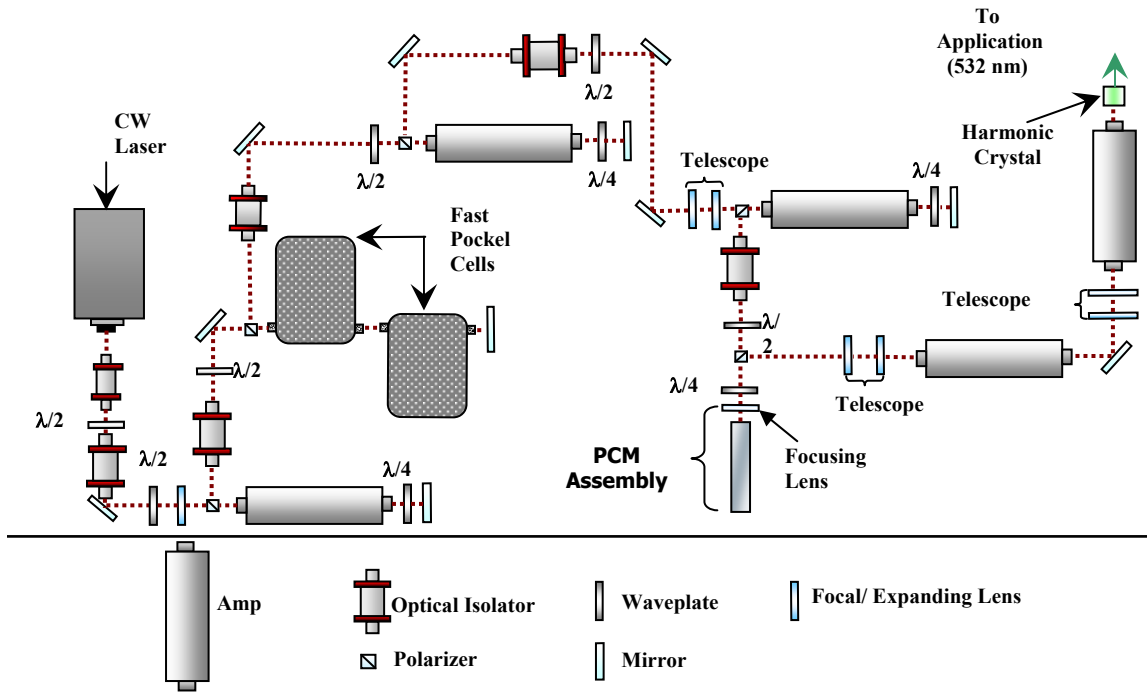


Figure 1: Schematic Diagram of Pulse Burst Laser

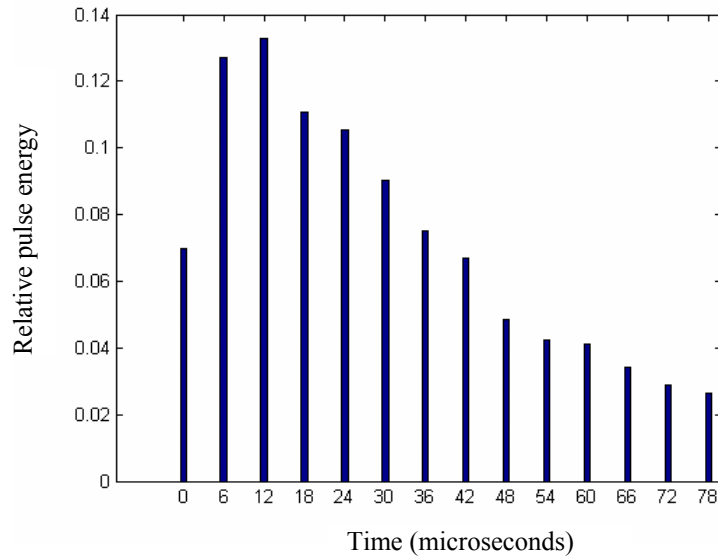


Figure 2 – Laser power distribution over burst of 14 pulses.

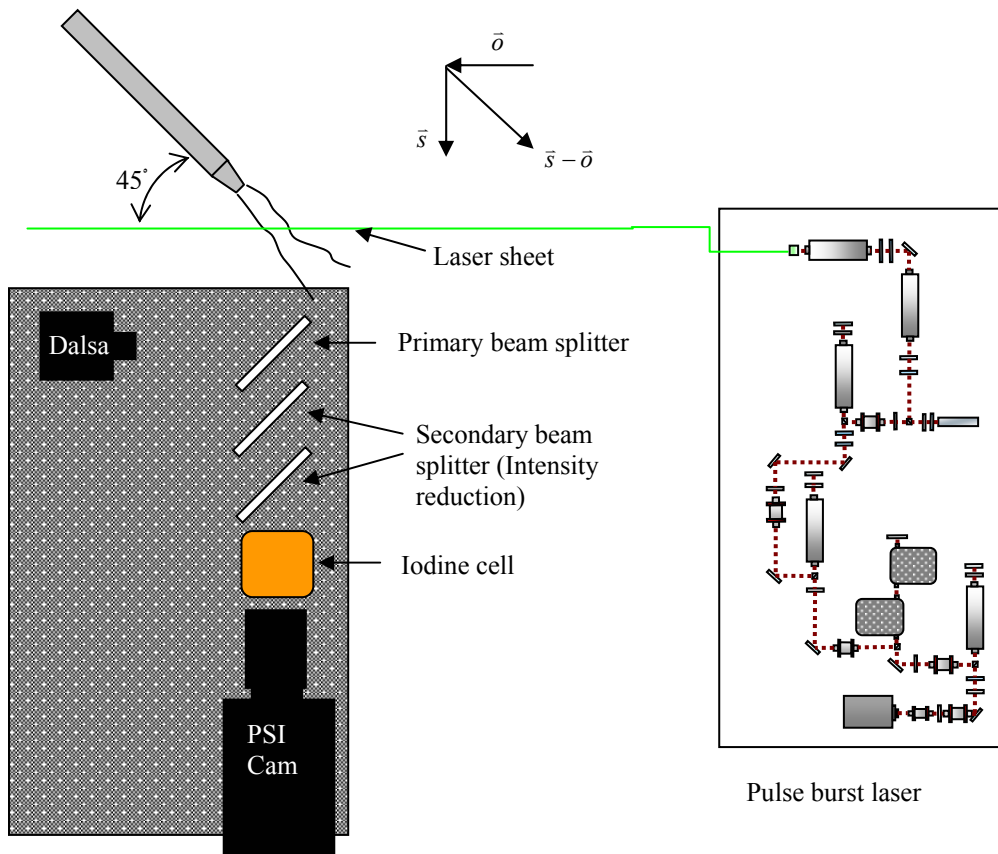


Figure 3 – Schematic of real-time PDV experiment.

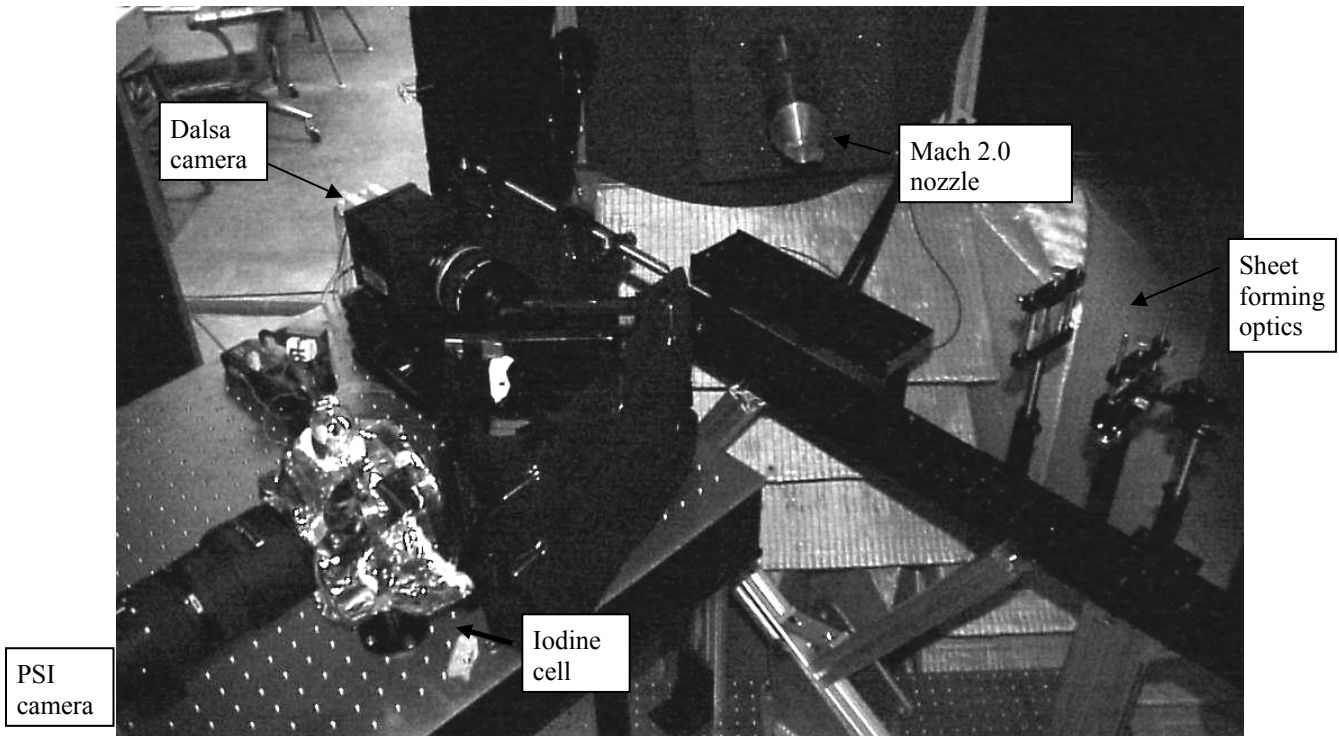


Figure 4 – Picture of real-time PDV experiment.

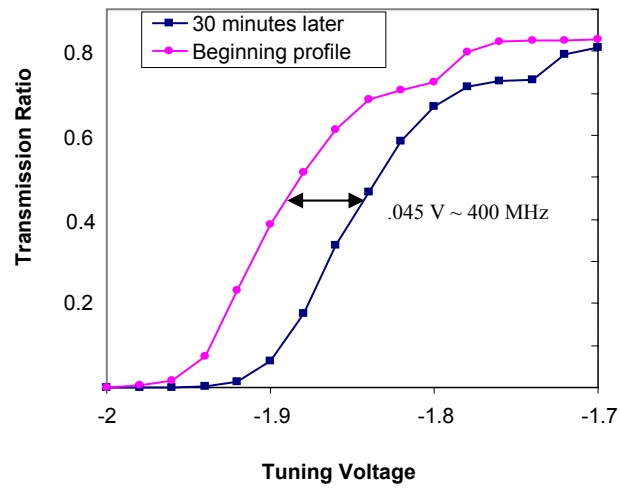


Figure 5 – Measured filter profiles using pulse burst laser.

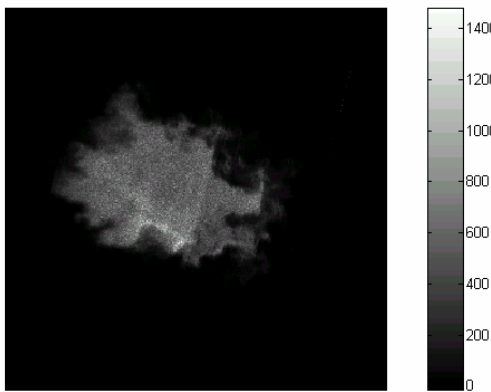


Figure 6 – Raw image of jet from Dalsa camera.

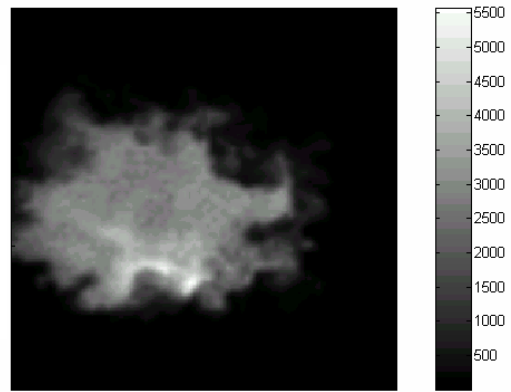


Figure 7 – Raw image of jet from PSI camera.

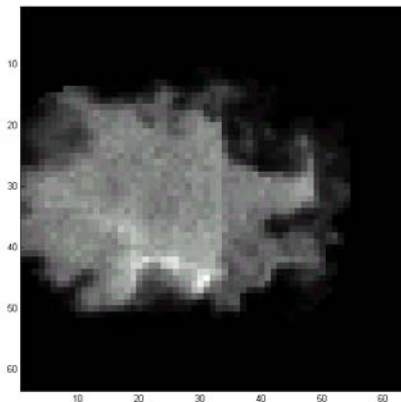


Figure 8 – Mapped image from Dalsa camera

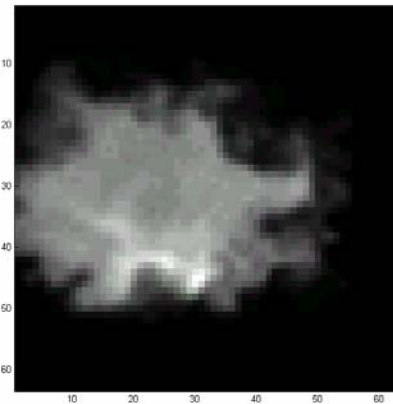


Figure 9 – Mapped image of jet from PSI camera.

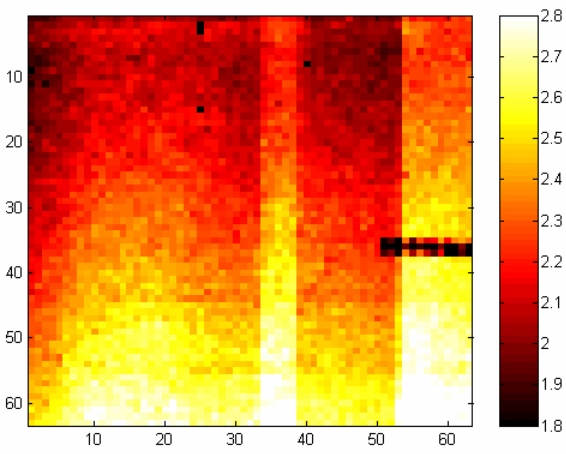


Figure 10 – Flat field calibration slope.

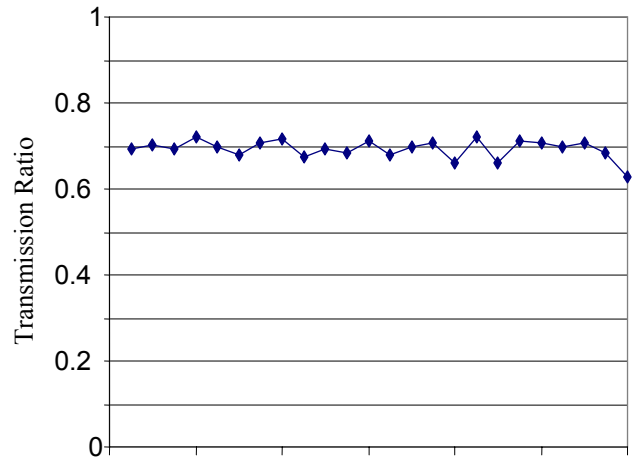


Figure 11 – Burst to burst frequency jitter of laser.

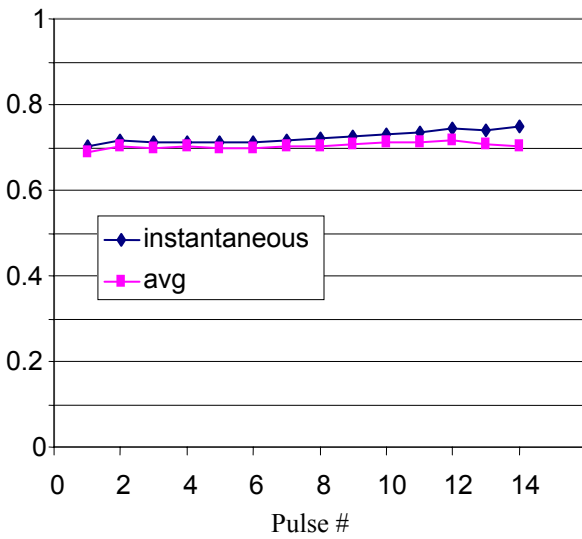


Figure 12 – Pulse to pulse jitter within a single burst.

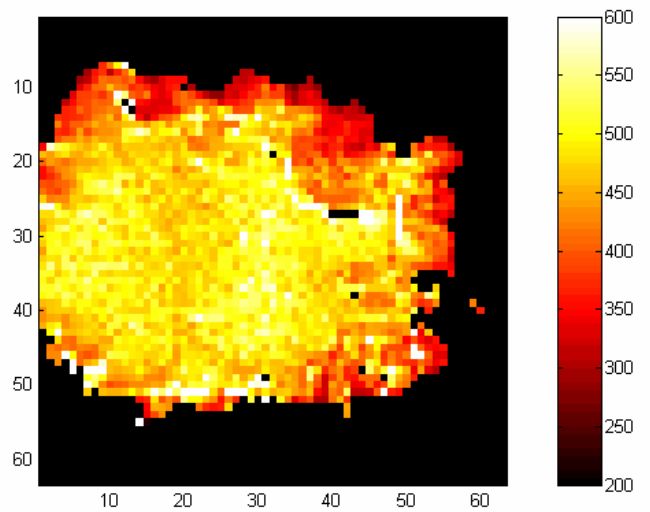


Figure 13 – Instantaneous velocity image.

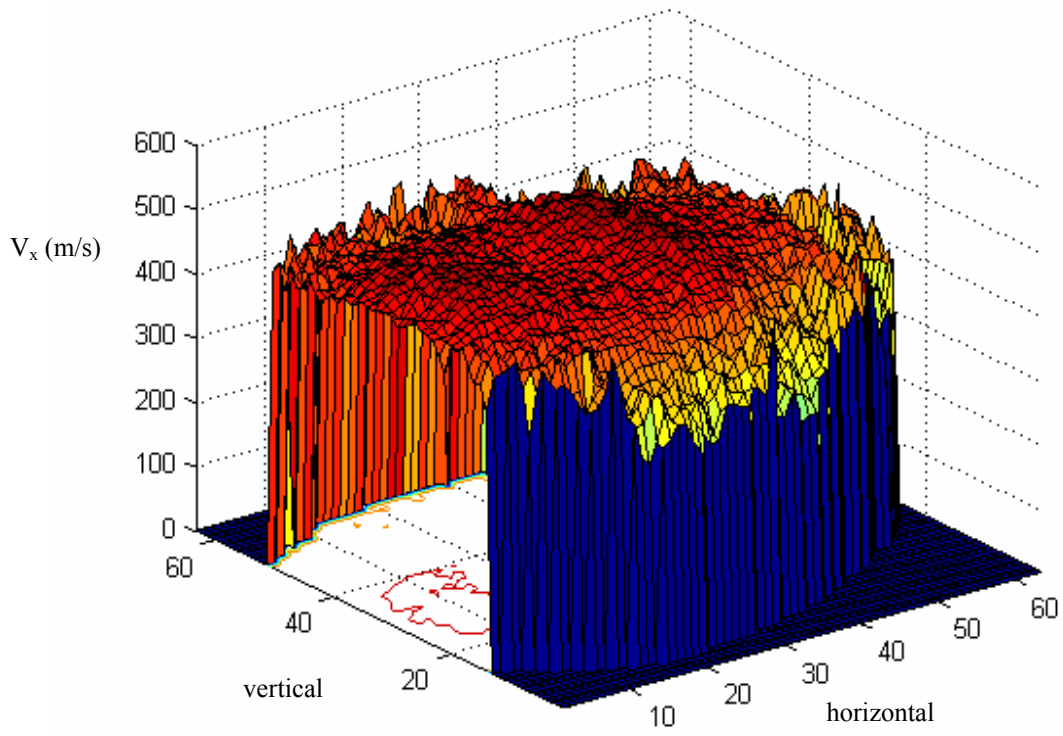


Figure 14 – Average velocity plot.

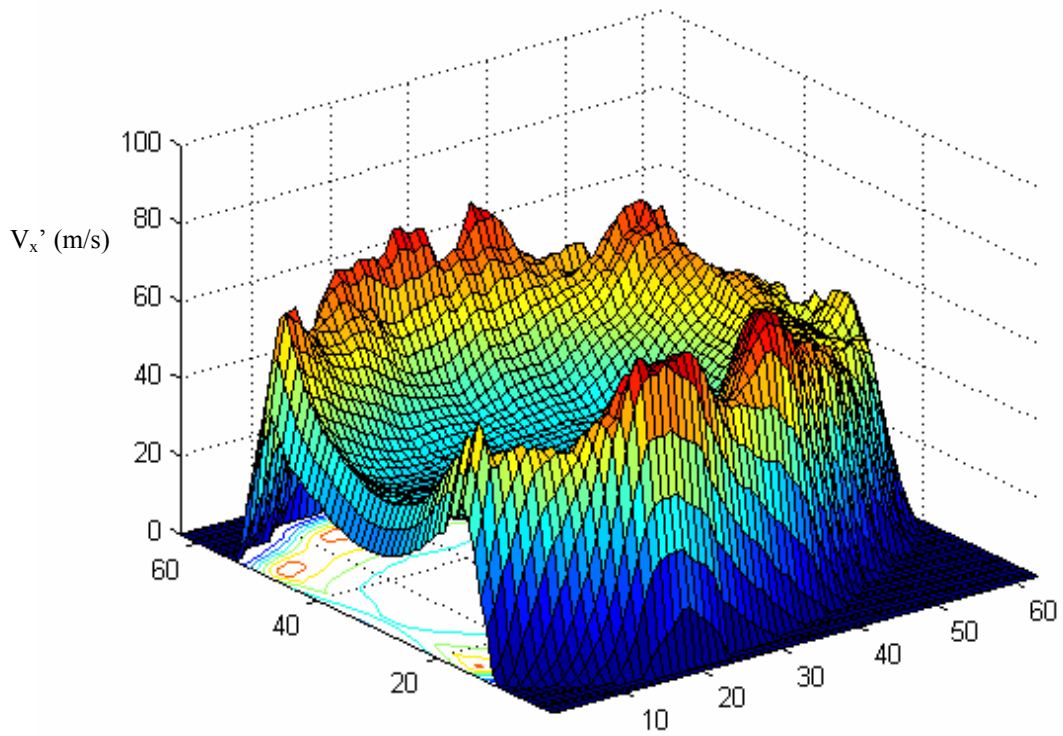


Figure 15 – Surface plot of velocity fluctuations.